Journal of
NANOSTRUCTURES
JNS
NANOSTRUCTURES
JNS.kashanu.ac.ir

Spinel-Type Cobalt Oxide (Co_3O_4) Nanoparticles from the mer-$Co(NH_3)_3(NO_2)_3$ Complex: Preparation, Characterization, and Study of Optical and Magnetic Properties

Saeed Farhadi*, Asma Sepahdar, Kosar Jahanara

Department of Chemistry, Lorestan University, Khoramabad 68135-465, Iran

Article history:
Received 12/5/2013
Accepted 11/8/2013
Published online 1/9/2013

Keywords:
Spinel–type cobalt oxide
Nanoparticles
Thermal decomposition
Co(III)-ammine complex
Ferromagnetic order

**Corresponding author:*
E-mail address:
sfarhadi48@yahoo.com
Phone: +98 6616200111
Fax: +98 6616200112.

Abstract

In this paper, the *mer*-$Co(NH_3)_3(NO_2)_3$ complex was used as a new precursor for synthesizing spinel-type cobalt oxide nanoparticles (Co_3O_4NPs).Thermal decomposition of the complex at low temperature (175 °C) resulted in the Co_3O_4NPs without using expensive and toxic solvents or complicated equipment. XRD, FT-IR, SEM, EDX, and TEM were employed to characterize the product, and its optical and magnetic properties were studied by UV-visible spectroscopy and a VSM, respectively. FT-IR, XRD and EDS analyses confirmed the formation of single-phase Co_3O_4 with cubic structure. The lattice constant calculated from XRD peaks is 8.0650 Å. SEM and TEM images showed that Co_3O_4NPs have a sphere-like morphology with an average size of 19 nm. Optical spectrum of Co_3O_4NPs revealed the presence of two band gaps at 2.20 and 3.45 eV values, which in turn confirmed the semiconducting properties. The magnetic measurement of Co_3O_4NPs showed a weak ferromagnetic order at room temperature.

1. Introduction

Transition-metal oxides nanoparticles exhibit novelproperties that significantly differ from those of corresponding bulk solids due to small size effect [1]. Among them, spinel-type cobalt oxide nanoparticles (Co_3O_4NPs) have attracted considerable attention owing to their unique properties and potential applications in gas sensors [2-3], heterogeneous catalysts [4-6], electrochemical devices [7], Li-ion batteries [8-11], magnetic materials [12, 13] and photocatalysts [14,15]. In recent years, the increasing interest has been focused on the synthesis of Co_3O_4 nanomaterials with unique size and specific shape because of the influences of particle size and morphology on their properties and applications [16-26]. Various chemical and physical routes to

synthesize Co_3O_4NPs have been reported such as hydro-/solvothermal method [27,28], combustion method [29-31],microwave heating [32-34], sol–gel process [35], spray pyrolysis [36], sonochemical method [37], coprecipitation [38], ionic liquid-assisted method [39], polyol method [40] and a non-aqueous route [41]. Nevertheless, most of these methods utilize complex processes, high calcination temperatures, and expensive and toxic reagents. In addition, they are either time consuming or require expensive instruments.

One of the most promising techniques to overcome the above mentioned problems is thermal decomposition of molecular precursors. This simple technique offers several unique advantages and significant merits over other methods including easy workup, short reaction time, and production of various inorganic nanomaterials with narrow size distribution [42-46]. In this context, several cobalt coordination compounds such as $CoC_2O_4.2H_2O$ [47], $[Co(Pht)(H_2O)]_n$ polymer [48], Co(salophen) [49], $Co(C_6H_5COO)(N_2H_4)_2$ [50], $[Co(NH_3)_5(OCO_2)](NO_3)_2$ [51], and $[Co(NH_3)_6](NO_3)_3$ [52]have been used to synthesize Co_3O_4 NPs via the thermal decomposition route. However, the search for more suitable precursors to synthesize Co_3O_4 nanoparticles at low temperature is still of great significance.

In the present work, we report a simple and low temperature routeto synthesizeCo_3O_4NPsvia direct thermal decomposition of the mer-$Co(NH_3)_3(NO_2)_3$ complex as a new precursor without employing solvent, surfactant and complicated equipment. The product was characterized by X-ray diffraction (XRD), Fourier transform infrared spectroscopy (FT-IR), scanning electron microscopy (SEM), energy-dispersive X-ray spectroscopy (EDS),transmission electronmicroscopy (TEM), UV-visible spectroscopy, and magnetic measurements.

2. Experimental procedure

2.1. Characterization techniques

The composition and phase purity of the as-prepared product was determined using a Rigaku D/max C III X-ray diffractometer using Ni-filtered Cu Ka radiation (λ = 1.5406 Å). XRD patterns were recorded in the 2θ range of 10°–80° with a scanning step of 0.02°.To investigate chemical bonding of the compounds, infrared spectra were recorded on the diluted samples in KBr pellets using a Schimadzu 160 FT–IR spectrophotometer in the rangeof 4000–400 cm^{-1}.Optical absorption spectra were recorded on a Shimadzu 1650PC UV–vis spectrophotometer in the 200–700 nm wavelength rangeat room temperature. The samples for UV-vis studies were well dispersed in distilled water by sonication for 30 min to form a homogeneous suspension. The morphology and particle size distribution of the as-prepared product were observed and scanning electron microscope (SEM, Philips XL-30SEM) at an accelerating voltage of 20 kV equipped with an energy dispersive X-ray spectroscopy and a transmission electron microscope (TEM, Philips CM10). For the TEM measurements, the powders were ultrasonicated in ethanol and a drop of the suspension was dried on a carbon-coated microgrid. The magnetic properties of Co_3O_4NPs were measured using a vibrating sample magnetometer (VSM, Iran MeghnatisDaghighKavir Company).

2.2. Preparation of Co_3O_4 NPs

The precursor complex, mer-$Co(NH_3)_3(NO_2)_3$, was synthesized according to the literature method [53] and its composition was confirmed by elemental analysis, and FT-IR. *Anal. Calc.* for mer-$Co(NH_3)_3(NO_2)_3$: Co, 23.80; H, 3.63; N, 33.88. Found: Co, 23.10; H, 3.65; N, 33.72.To prepare Co_3O_4NPs, an appropriate amount of the complex powder (1 to 2 g) was added to a porcelain crucible

and was then transferred into a muffle furnace. The sample was heated at the rate of 10 ◦C min^{-1} from room temperature to 150 ˚C in air atmosphere and was maintained at this temperature for 1 h. Similar experiment was performed for the sample calcined at 175 ◦C. The decomposition productgenerated from the complex at each temperature was collected for characterization.

3. Results and discussion

XRD patterns of the decomposition products of the complex at150 and 175 °C are shown in Fig. 1. For the complex sample heated at 150 °C (Fig. 1(a)), besides peaks belonged to cubic Co_3O_4NPs, some peaks related to the face center cubic CoO phase (JCPDS card 43-1004) appeared which marked by "Δ" in the pattern. As can be seen in Fig. 1(b), all peaks (111), (220), (311), (222), (400), (422), (511), (440), (620) and (533) appeared for thesample calcined at 175°C could be indexed to the face centered-cubic phase of spinel Co_3O_4, in agreement with the literature values (JCPDS card file no. 76-1802). At this temperature, no diffraction peaks related toCoO and other impurity phases are observed, indicating the complete decomposition of the precursor into pure Co_3O_4 phase. The XRD results also reveal that the intensity of the characteristic peaks of the Co_3O_4 increases with temperature, indicating that the crystallinity of the Co_3O_4 becomes higher with increasing calcination temperature. As can be seen, the diffraction peaks are markedly broadened due to the small size effect of the nanoparticles.The average particle size was estimated from the X-ray line broadening of the diffraction peaks using the Scherrer relation [54]: D= 0.9λ/(Bcosθ), where λ is the wavelength of Cu Kα radiation, B is the corrected full-width at half-maximum (FWHM) of the diffraction peak and θ is the Bragg angle. As can be seen in Table 1, the crystallite sizes of the Co_3O_4phase calculated based on the FWHM of the diffraction peaks are in the range of 14 to 26 nm. From these data, the mean size of particles is estimated to be approximately 18.83 nm. The lattice parameter constant (a_0) of Co_3O_4 NPs were determined using the following relationship.

$$a_0 = d_{hkl} (h^2 + k^2 + l^2)^{1/2}$$

The a_0 calculated from the XRD pattern is 8.0650 Å which is close to the literature value (JCPDS card file no. 76-1802).

Table 1. The crystallite sizes of Co_3O_4phase calculated based on the FWHM of some diffraction peaks.

No.	Position [°2Th.]	(hkl)	d_{hkl} [Å]	FWHM [°2Th.]	Particle size (D; nm)
1	31.48	220	2.85	0.4723	17.29
2	37.11	311	2.43	0.4723	17.18
3	38.83	222	2.33	0.5904	14.16
4	59.62	511	1.55	0.4723	19.18
5	65.43	440	1.43	0.3542	26.38

Average crystallite size ≈ 18.83 nm.

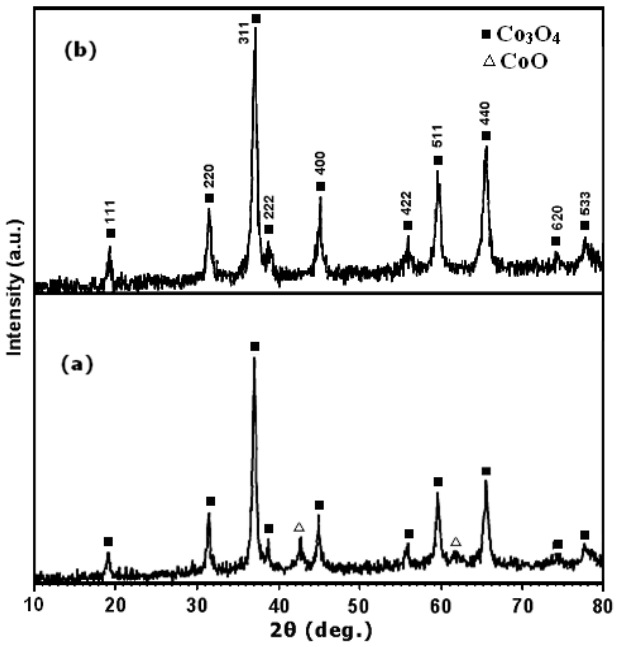

Fig. 1. XRD patterns of the decomposition products of the $Co(NH_3)_3(NO_2)_3$ complex at:(a) 150 °C and (b) 175 °C.

FT-IR spectra of the mer-$Co(NH_3)_3(NO_2)_3$ complex and its decomposition products are shown in Fig. 2. For the complex in Fig. 2(a), the characteristic bands of NH_3ligand are observed at approximately 3500-3000, 1600-1500, 1050 cm^{-1} and bands of the -NO_2 ligand appeared at 1450-1250 and 650cm^{-1} [55]. For the complex sample heated at 150 °C as shown in the Fig. 2(b), most of the bands associated with the complex disappeared and two characteristic bands of the spinel-type Co_3O_4 structure at 661.54 (υ_1) and 566.10 (υ_2) cm^{-1} are observed [32]. The $\upsilon_1$band is characteristic of Co^{3+}–O vibration in an octahedral site, and the υ_2 band is attributable to the Co^{2+}–O vibration in a tetrahedral site of the Co_3O_4 lattice. As can be seen in Fig. 2(c), for the sample calcined at 175 °C only two characteristic bands of the Co_3O_4 phase are observed, confirming complete decomposition of the complex to the Co_3O_4 phase as indicated by the XRD results.

The morphology of the product was investigated by SEM. Fig. 3 shows the SEM images of Co_3O_4 NPs in two different magnifications. From the SEM images, it is clearly evident that the sample consists of sphere-like fine particles which were loosely aggregated. It seems that the particles are size-homogeneous and appreciably dispersed. It could be concluded that this preparation method has successfully overcame the problem of agglomeration and is appropriate to obtain the Co_3O_4 NPs with smaller size. Since it is very difficult to measure the exact size of particles by SEM, we used TEM analysis to ascertain the physical nature of the Co_3O_4 NPs. Fig. 4 shows TEM image of the Co_3O_4 powder prepared by thermal decomposition of the mer-$Co(NH_3)_3(NO_2)_3$ complex at 175 °C. The TEM sample was prepared by dispersing the powder in ethanol by ultrasonic vibration. The Co_3O_4particles have sphere-like shapes with weak agglomeration. The size distribution of Co_3O_4 NPs has also been determined from the TEM image. The size distribution of the Co_3O_4NPshas also been investigated from the particles visualized under TEM analysis. The particle size histogram was determined by counting more than 100 particles in randomly selected regions on the TEM copper grid. The histogram based on TEM analysis is shown in the inset of Fig.4. From the inset, it can be seen that the nanoparticles possess a narrow size distribution in the range of 14to26 nm, and the mean particle diameter is approximately 19 nm which is very close to the average size calculated by the Scherrer relation.

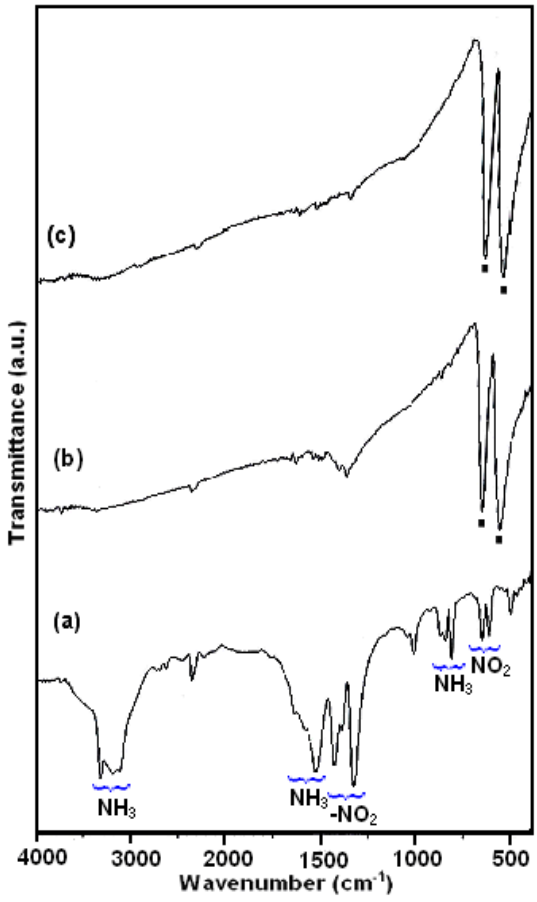

Fig. 2. FT-IR spectra of (a) the$Co(NH_3)_3(NO_2)_3$ complex and its decomposition products at (b) 150 °C and (c) 175 °C.

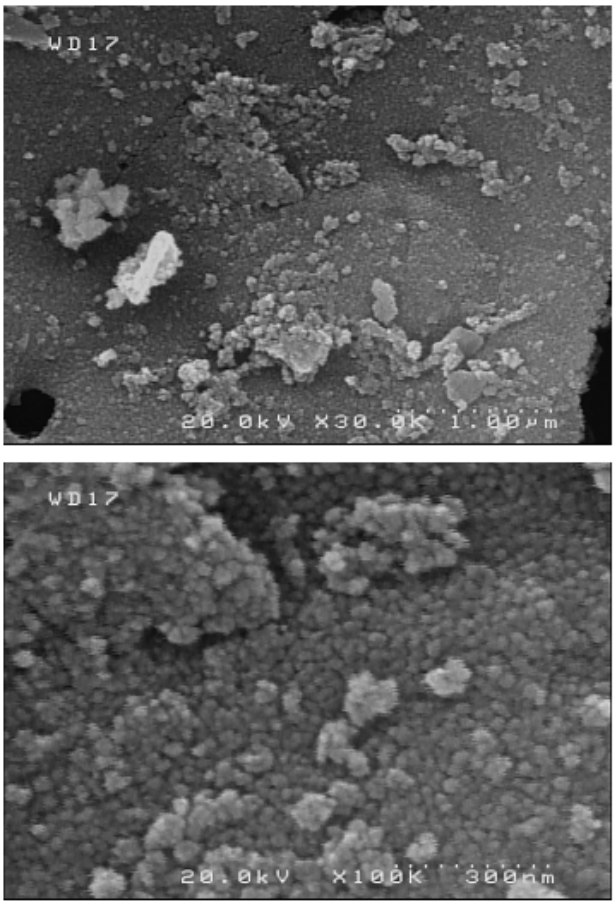

Fig. 3. SEM images of the Co_3O_4 nanoparticles prepared from the decomposition of the mer-$Co(NH_3)_3(NO_2)_3$complex at175 °C.

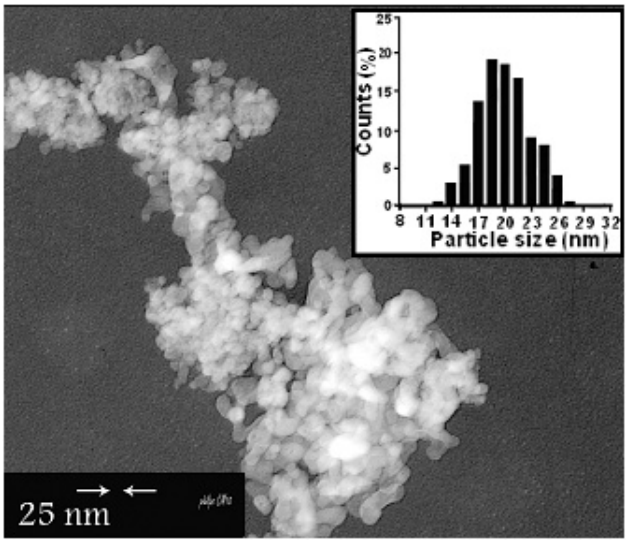

Fig. 4. TEM image of the Co_3O_4 nanoparticles prepared from the decomposition of the mer-$Co(NH_3)_3(NO_2)_3$complex at175°C.

Energy dispersive X-ray spectrometry (EDX) analysis was employed to determine the composition of the Co_3O_4 NPsprepared at175 °C. As shown in Fig. 5, the EDX spectrum of the product contains only oxygen and cobalt elements. No other elements can be detected in the spectrum, indicating high purity of the Co_3O_4 nanoparticles. The experimental atomic percentages of Co and O are found to be 43.22% and 56.78%, respectively, which is near to the theoretical ratio (3:4) of Co_3O_4.

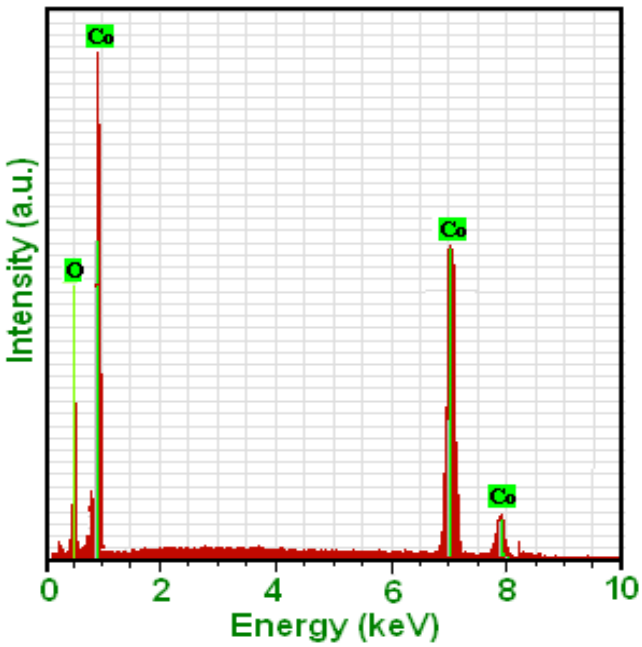

Fig. 5. EDX spectrum of the Co_3O_4 nanoparticles prepared at 175 °C.

The optical absorption properties of the as-prepared Co_3O_4 NPs were investigated at room temperature by UV–vis spectroscopy. As can be seen in Fig. 6, two absorption bands appear in 200–360 and 380–600 nm wavelength ranges. As has been reported in the literatures [16,30], the first absorption band can be assigned to the O^{2-}toCo^{2+} charge transfer process while the second one to the O^{2-}toCo^{3+} charge transfer. Co_3O_4 is a p-type semiconductor and the absorption band gap E_g can be determined by the following

equation: $(\alpha h\nu)^n = K(h\nu - E_g)$,where h$\nu$ is the photo energy, α is the absorption coefficient, K is a constant relative to the material, and n is either 2 for a direct transition or 1/2 for an indirect transition. Here n is 2 for Co_3O_4 NPs sample. The plot of $(\alpha h\nu)^2$ versus $h\nu$ is shown in the inset of Fig. 6. The value of hν extrapolated to $(\alpha h\nu)^2 = 0$ gives an absorption band gap energy (E_g). The absorption bands in Fig. 6 yield two E_g values of 3.45 and 2.20 eV for the sample which are blue-shifted relative to reported values for the bulk sample (2.19 and 1.48 eV, respectively) [56]. The increase in the band gaps of the Co_3O_4 NPs may ascribe to the quantum confinement effects of nanoparticles.

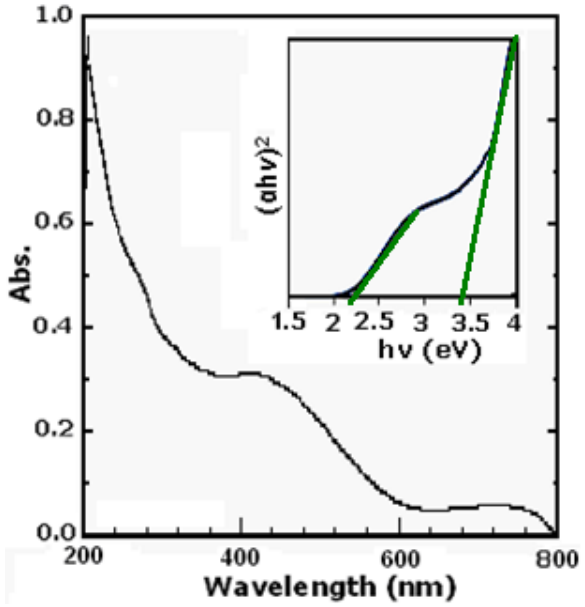

Fig. 6. UV-Visspectrum and $(Ah\nu)^2$-hν curve (inset) of the$Co_3O_4Co_3O_4$nanoparticles prepared at 175 °C.

Room-temperature magnetic measurements of the Co_3O_4 NPs prepared at 175°Care shown in Fig. 7. Fig 7(a) shows that the magnetization curve versus the applied magnetic field is approximately linear with a fine hysteresis loop. From Fig. 7(b), the coercive field and the remanent magnetization are estimated to be approximately 135Oe and 0.05emu/g, respectively. The maximum field applied (8 kOe) does not saturate the magnetization, and the magnetization at this applied field is approximately 0.35 emu/g. The low coercive field and remanent magnetization confirm that the Co_3O_4 nanoparticles exhibit a weak ferromagnetic order. This behavior is similar to that of Co_3O_4 NPs obtained by previously reported methods [47,48,57] and may be explained by uncompensated surface spins and/or finite size effects of the Co_3O_4 NPs [58].

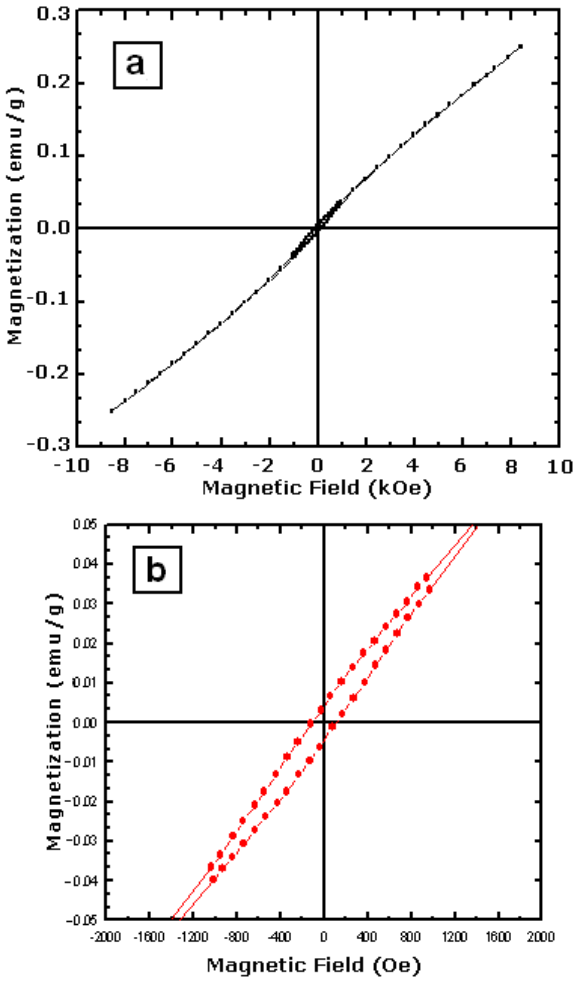

Fig. 7. (a) Magnetization curve as a function of applied magnetic field for Co_3O_4 nanoparticles at room temperature and (b) the expansion of magnetization vs. field near the lower applied field.

In Table 2, we have compared the reaction conditions and some physical properties of Co_3O_4 NPs

obtained in the present method with some reported studies.From Table 2, it is clear that the present method is more suitable and/or superior to other methods with respect to the reaction conditions, reaction temperature and time, average particle size and particle size distribution.We can see that most of the reported methods are associated with one or more disadvantages such as long preparation times, high temperature requirement, use of expensive and/or toxic solvents and surfactants, and the formation of particles with large sizes and wide size distribution. By the present method, Co_3O_4 NPs with a narrow size distribution could be prepared at lower temperature without the use of solvent, surfactant and any expensive complicated equipment.

Table 2. Comparison of reaction conditions and properties of the Co_3O_4 nanoparticles prepared in the present work with some reported methods.

Entry	Method	Reaction conditions (solvent, and surfactants)	Temperature (°C)	Time (h)	Particle size (nm)	Ref.
1	Hydrothermal	Water, Polyvinylpyrrolidone.	150	16	350	[27]
2	Combustion	Water, urea	450-550	0.5	25	[30]
3	Microwave irradiation	Ethylene glycol, Trioctyl phosphine oxide.	400	3	6	[34]
4	Sol-gel	Liquid N_2, Propionic acid	260	2	300	[35]
5	Sonochemical	Deoxygenated water or Water/DMF, Ar atmosphere, RT	Ultrasonic irradiation	3	30	[37]
6	Ionic-liquid assisted	[BMIM]OH[a]/H_2O_2/NaOH	RT	6	10-50	[39]
7	Polyol	ethylene glycol//PEG/	200	12	90-110	[40]
8	Thermal decomposition of $CoC_2O_4{\cdot}2H_2O$ nanorod	No solvent or surfactant	450	4	60	[46]
9	Thermal decomposition of [Co(Pht)(H_2O)]n	Oleic acid,Triphenylphosphine	220	1	20-30	[47]
10	Thermal decomposition of Co(salophen)	No solvent or surfactant	500	5	30-50	[48]
11	Thermal decomposition of $Co(C_6H_5COO)(N_2H_4)_2$	water	heating with a flame gently		20	[49]
12	Thermal decomposition of $[Co(NH_3)_6](NO_3)_3$	No solvent or surfactant	200	1	15	[51]
13	Thermal decomposition of mer-$Co(NH_3)_3(NO_2)_3$	No solvent or surfactant	175	1	19	This work

[a][BMIM]OH = 1-n-Butyl-3-methylimidazolium hydroxide (an ionic liquid).

4. Conclusions

In conclusion, Co_3O_4 NPs with an average particle size of 19 nm have been successfully prepared via the thermal decomposition of the mer-$Co(NH_3)_3(NO_2)_3$ at 175 °C. The Co_3O_4 NPs are formed from this complex via a redox reaction between NH_3 and the NO_2^- ions. This method yields sphere-like Co_3O_4 NPs with a narrow size distribution and weak ferromagnetic behavior. The estimated optical absorption band gaps of the Co_3O_4 NPs are relatively blue-shifted, compared to the values for the bulk sample. This approach provides a one-step simple and inexpensive route for the preparation of high-purity Co_3O_4 NPs for the industrial and high-technology applications.

Acknowledgement

The authors are grateful to the Lorestan University Research Council and Iran Nanotechnology Initiative Council (INIC) for their financial supports.

References

[1] K.J. Klabunde, R.M. Richards, Nanoscale Materials in Chemistry, 2nd ed., Wiley, New York, 2012.

[2] W.-Y. Li, L.-N. Xu, J. Chen, Adv. Funct. Mater. 15 (2005) 851–857.

[3] R. Wu, J. Wu, M. Yu, T. Tsai, C. Yeh, Sens. Actu. B: Chem. 131 (2008) 306-312.

[4] A. Askarinejad, M. Bagherzadeh, A. Morsali, Appl. Surface Sci. 256 (2010) 6678–6682.

[5] T.E. Davies, T. Garcia, B. Solsona, S.H. Taylor, Chem. Commun. 32 (2006) 3417–3419.

[6] V.R. Mate, M. Shirai, C.V. Rode, Catal. Commun. 33 (2013) 66-69.

[7] T. Maruyama, S. Arai, J. Electrochem. Soc. 143 (1996) 1383-1386

[8] N. Du, H. Zhang, B.D. Chen, J.B. Wu, X.Y. Ma, Z.H. Liu, Y.Q. Zhang, D.R. Yang, X.H. Huang, J.P. Tu, Adv. Mater. 19 (2007) 4505–4509.

[9] X.W. Lou, D. Deng, J.Y. Lee, L.A. Archer, Adv. Mater. 20 (2008) 258–262.

[10] S.-L. Chou, J.-Z. Wang, H.-K. Liu, S.-X. Dou, J. Power Sources 182 (2008) 359–364.

[11] Y.G. Li, B. Tan, Y.Y. Wu, Nano Lett. 8 (2008) 265–270.

[12] R.M. Wang, C.M. Liu, H.Z. Zhang, C.P. Chen, L. Guo, H.B. Xu, S.H. Yang, Appl. Phys. Lett. 85 (2004) 2080-2082.

[13] S.A. Makhlouf, J. Magn. Magn. Mater. 246 (2002) 184–190.

[14] X. Lou, J. Han, W. Chu, X. Wang, Q. Cheng, Mater. Sci. Eng. B 137 (2007) 268–271.

[15] T. Warang, N. Patel, A. Santini, N. Bazzanella, A. Kale, A. Miotello, Appl. Catal. A: Gen. 423– 424 (2012) 21– 27.

[16] L. Sun, H. Li, L. Ren, C. Hu, Solid State Sci. 11 (2009) 108–112.

[17] Y. Chen, Y. Zhang, S. Fu, Mater. Lett. 61, (2007) 701–705.

[18] T. Lai, Y. Lai, C. Lee, Y. Shu, C. Wang, Catal. Today 131, (2008) 105–110.

[19] W.W. Wang, Y.J. Zhu, Mater. Res. Bull. 40, (2005) 1929–1935.

[20] L. Li, Y. Chu, Y. Liu, J.L. Song, D. Wang, X.W. Du, Mater. Lett. 62, (2008) 1507–1510.

[21] J. Du, L. Chai, G. Wang, K. Li, Y. Qian, Aust. J. Chem. 61, (2008) 153–158.

[22] R.M. Wang, C.M. Liu, H.Z. Zhang, C.P. Chen, L. Guo, H.B. Xu, S.H. Yang, Appl. Phys. Lett. 85 (2004) 2080–2082.

[23] Y. Li, J. Zhao, Y. Dan, D. Ma, Y. Zhao, S. Hou, H. Lin, Z. Wang, Chem. Eng. J. 166 (2011) 428–434.

[24] H. Sun, M. Ahmad, J. Zhu, Electrochim. Acta 89, (2013) 199– 205.

[25] M. Ren, S. Yuan, L. Su, Z. Zhou, Solid State Sci. 14 (2012) 451-455.

[26] L.X. Yang, Y.J. Zhu, L. Li, L, Zhang, H. Tong, W.W. Wang, Eur. J. Inorg. Chem. 23 (2006) 4787–4792.

[27] J. Ma, S. Zhang, W. Liu, Y. Zhao, J. Alloys Compd. 490 (2010) 647–651.

[28] E. Lester, G. Aksomaityte, J. Li, S. Gomez, J. Gonzalez-Gonzalez, M. Poliakoff, Prog. Cryst. Growth Charact. Mater. 58 (2012) 3–13.
[29] J. Jiu, Y. Ge, X. Li, X, L. Nie, Mater. Lett. 54 (2002) 260–263.
[30] F. Gu, C. Li, Y. Hu, L. Zhang, J. Cryst. Growth 304 (2007) 369–373.
31. M.C. Gardey-MerinO, M. Palermo, R Belda, M.E. Fernández de Rapp, G.E.Lascalea, P.G. Vázquez, Proced. Mater. Sci. 1 (2012)588–593.
[32] L.-H. Ai, J. Jiang, Powder Tech. 195 (2009) 11–14
[33] L. Li, J. Ren, Mater. Res. Bull. 41 (2006) 2286–2290.
[34] A.S. Bhatt, D.K. Bhat, C.-W. Tai, M.S. Santosh, Mater. Chem. Phys. 125 (2011) 347–350.
[35] M.E. Baydi, G. Poillerat, J.L. Rehspringer, J.L. Gautier, J.F. Koenig, P. Chartier, J. Solid State Chem. 109 (1994) 281–288.
[36] D.Y. Kim, S.H. Ju, H.Y. Koo, S.K. Hong, Y.C. Kangf, J. Alloys Compd. 417 (2006) 254–258.
[37] R.V. Kumar, Y. Diamant, A. Gedanken, Chem. Mater. 12 (2000) 2301–2305.
[38] K. Sinko, G. Szabo, M. Zrinyi, J. Nanosci. Nanotechnol. 11 (2011) 1–9.
[39] D. Zou, C. Xu, H. Luo, L. Wang T.Ying, Mater. Lett. 62 (2008) 1976–1978.
[40] J. Jiang, L. Li, Mater. Lett. 61(2007) 4894–4896.
[41] S. Fan, X. Liu, Y. Li, E. Yan, C. Wang, J. Liu, Y. Zhang, Mater. Lett. 91 (2013) 291–293
[42] E. Traversa, M. Sakamoto, Y. Sadaoka, Part. Sci. Technol. 16 (1998) 185–214.
[43] S. Farhadi, N. Rashidi, Polyhedron 29 (2010) 2959–2965.
[44] S. Farhadi, Z. Roostaei-Zaniyani, Polyhedron 30 (2011) 1244–1249.
[45] M.Y. Masoomi, A. Morsali, Coord. Chem. Rev. 256 (2012) 2921-2943
[46] L. Ren, P. Wang, Y. Han, C. Hu, B. Wei, Mater. Phys. Lett. 476 (2009) 78–83.
[47] F. Mohandes, F. Davar, M. Salavati-Niasari, J. Magn. Magn.Mater.322 (2010) 872–877.
[48] M. Salavati-Niasari A. Khansari, F. Davar, Inorg. Chim. Acta 362 (2009) 4937–4942
[49] K. Thangavelu, K. Parameswari, K. Kuppusamy, Y. Haldorai, Mater. Lett. 65 (2011) 1482–1484
[50] S. Farhadi, J. Safabakhsh, J. Alloys Compd. 515 (2012) 180–185.
[51] S. Farhadi, K. pourzare, Mater. Res. Bull. 47 (2012) 1550-1556.
[52] H. Yan, X. Xie, K. Liu, H. Cao, X. Zhang, Y.Luo, Powder Tech. 221 (2012) 199–202.
[53] K. Wieghardt, H. Siebert, Inorg. Synth. 23 (1985) 107-110.
[54] H.P. Klug, L.E. Alexander, X-ray Diffraction Procedures, 2nd ed., Wiley, New York, 1964.
[55] K. Nakamoto, Infrared and Raman Spectra of Inorganic and Coordination Compounds, Part B: Applications in Coordination, Organometallic, and Bioinorganic Chemistry, sixth ed., Wiley, New York, 2009.
[56] B. Varghese, T.C. Hoong, Z. Yanwu, M. V. Reddy, B. V.R. Chowdari, A.T.S. Wee, T.B.C. Vincent, C.T. Lim, C.-H. Sow, Adv. Funct.Mater. 17 (2007) 1932-1939.
[57] Y. Qi, Y. Zhao, Z. Wu, Mater. Chem. Phys. 110 (2008) 457-462.
[58] X.P. Shen, H.J. Miao, H. Zhao, Z. Xu, Appl. Phys. A: Mater. Sci. Process 91 (2008) 47-51.